RSC Advances

PAPER

View Article Online
View Journal | View Issue

Cite this: *RSC Adv.*, 2025, **15**, 34733

Evaluation of alginate/poly(vinyl alcohol)/$BaSO_4$ hydrogels for nucleus pulposus regeneration

Amaliya Rasyida,[a] Dindra Fai'mundiarti Purnamabroto,[a] Agung Purniawan,[a] Indra Carllistya Pramadio,[a] Femiana Gapsari[b] and Adelina Salsabila Ednanda[a]

Received 17th June 2025
Accepted 10th August 2025

DOI: 10.1039/d5ra04291g

rsc.li/rsc-advances

Intervertebral disc degeneration is a major contributor to lower back pain worldwide, underscoring the urgent need for effective, minimally invasive regenerative therapies. One of the critical challenges in nucleus pulposus (NP) replacement lies in developing injectable hydrogels with optimal gelation behavior, radiopacity, mechanical properties, and biocompatibility. This study investigates the influence of varying concentrations of Na_2HPO_4 (0.3%, 0.4%, 0.5%) and $BaSO_4$ (1%, 1.5%) in ALG/PVA hydrogels through a series of gelation time measurements, radiopacity analysis, mechanical testing, and *in vitro* biocompatibility assays. The optimal formulation, containing 1.5 wt% $BaSO_4$ and 0.4 wt% Na_2HPO_4, achieved a gelation time of 12.5 ± 0.5 minutes, radiopacity of 71–74%, elastic modulus of 0.055 ± 0.015 MPa, and cell viability above 90%, fulfilling key criteria for NP scaffold performance. Although compressive strength remained below physiological requirements, the formulation demonstrated excellent injectability, structural integrity, and biological response. This study offers a novel strategy by combining retarding and radiopaque agents in a single hydrogel system, contributing to the advancement of injectable biomaterials for intervertebral disc regeneration.

Introduction

Spinal disorders are a growing public health concern, affecting over 632 million people globally and exerting a substantial socio-economic burden due to their chronic nature and high treatment costs. Among these conditions, lower back pain is the most prevalent, commonly caused by degenerative disc disease (DDD) or intervertebral disc degeneration (IVD). The intervertebral disc (IVD) is composed of three main structural components: the nucleus pulposus (NP) at the center, which provides hydration and mechanical cushioning; the surrounding annulus fibrosus (AF), which provides tensile strength; and the cartilage endplate (CEP), which facilitates nutrient transport. The NP plays a critical role in maintaining spinal flexibility and load distribution. Degeneration of this gelatinous tissue can lead to reduced disc height, structural instability, nerve compression, chronic pain, and limited mobility. Lower back pain emerges as a complex and multifactorial condition, driven by anatomical degeneration, age-related changes, and lifestyle factors, necessitating effective regenerative strategies[1–4]

Historically, the concept of NP replacement was introduced in the 1960s by Nachemson,[5] who injected self-curing silicone into cadaveric discs. This approach evolved in the early 1990s when Bao and Higham[6] developed injectable hydrogels as biomimetic substitutes for NP. These materials have since gained traction due to their ability to conform to irregular defects, reduce implant migration, and minimize surgical invasiveness. The biological and mechanical criteria for successful NP replacement include biocompatibility, biodegradability, sufficient mechanical strength, controlled gelation time, and radiopacity. Injectable hydrogels now play a pivotal role in tissue engineering, acting as scaffolds that restore disc structure and function[7–9]

Nevertheless, several challenges hinder the clinical efficacy of injectable hydrogels for NP regeneration. Chief among these are their insufficient compressive strength (ideally ~1.0 MPa), unpredictable gelation kinetics, and a high risk of post-injection leakage. These issues can impair the integration and performance of hydrogels *in vivo*, particularly under the dynamic and pressurized conditions of the intervertebral disc. Hence, advanced hydrogels must exhibit finely tuned mechanical, biological, and radiological properties. A strategic approach involves incorporating retarding agents, such as Na_2HPO_4, to delay premature gelation, and radiopaque agents, such as $BaSO_4$, to improve visualization and placement accuracy during clinical procedures.[10–14]

Among potential biomaterials, alginate is widely recognized for its biocompatibility, biodegradability, and structural similarity to natural extracellular matrix (ECM), making it an ideal candidate for NP scaffold design. It supports cell proliferation and ECM synthesis under physiological conditions. When

[a]*Department of Materials and Metallurgical Engineering, Faculty of Industrial Technology and Systems Engineering, Institut Teknologi Sepuluh Nopember, Surabaya, 60111, Indonesia. E-mail: amaliya@its.ac.id*
[b]*University of Brawijaya, Malang, Indonesia*

combined with poly(vinyl alcohol) (PVA), a co-polymer known for its mechanical robustness, partial biodegradability, and good hydrogel-forming capacity, the resulting composite offers enhanced mechanical stability while retaining biological functionality. In this context, Na_2HPO_4 serves as a retarding agent to regulate ionic crosslinking between alginate and calcium ions, thus optimizing gelation time. Concurrently, $BaSO_4$ functions as a radiopaque additive, enabling radiological imaging during and after injection, thereby facilitating real-time monitoring and post-operative assessment.[15–17]

This study aims to systematically investigate the effects of varying Na_2HPO_4 (0.3%, 0.4%, and 0.5 wt%) and $BaSO_4$ (1% and 1.5 wt%) concentrations in ALG/PVA hydrogels, with specific focus on gelation time, radiopacity, porosity, swelling behavior, compressive strength, and biocompatibility. The novelty of this research lies in the dual incorporation of both retarding and radiopaque agents—a combination that has not been extensively explored in previous studies, which often examined these additives independently. The findings of this study are expected to contribute significantly to the development of optimized injectable hydrogel systems that meet the clinical requirements for NP regeneration, potentially improving therapeutic outcomes in patients with IVD degeneration and expanding the applications of these biomaterials in spinal tissue engineering.[18–30]

Experimental procedure

Materials and methods

Hydrogel synthesis. The ALG/PVA/$BaSO_4$ composite hydrogel was synthesized by dissolving poly(vinyl alcohol) (PVA) at concentrations of 20 wt% and 30 wt% in 40 mL of distilled water. The solution was stirred using a magnetic stirrer at 120 °C and 1000 rpm for 1 hour until complete dissolution was achieved. Once a homogeneous solution was obtained, $BaSO_4$ powder was added at 1 wt% and 1.5 wt% concentrations, followed by stirring for 10 minutes. Sodium alginate (SA) was then added at 80 wt% for the 20 wt% PVA group and 70 wt% for the 30 wt% PVA group, and the mixture was stirred at 250 rpm for 1 hour. Di-sodium hydrogen phosphate (Na_2HPO_4), pre-dissolved in 5 mL of distilled water, was added at concentrations of 0.3 wt%, 0.4 wt%, and 0.5 wt%, and stirred at 250 rpm for 45 minutes. Additionally, calcium sulfate ($CaSO_4$) powder (1 wt%) was dissolved in 5 mL of distilled water and stirred at 250 rpm for 45 minutes to form a $CaSO_4$ suspension.

Materials. The following reagents were used: sodium alginate (medium viscosity, 80–120 kDa), PVA (M_w = 60 000 g mol^{-1}), calcium sulfate ($CaSO_4$, M_w = 136.14 g mol^{-1}), Na_2HPO_4 (M_w = 177.99 g mol^{-1}), and $BaSO_4$ (M_w = 233.40 g mol^{-1}). Sodium alginate and PVA were sourced from Sigma-Aldrich (USA) and Merck (Germany), respectively; $CaSO_4$ from MaxLab (Indonesia); and both Na_2HPO_4 and $BaSO_4$ from SAP Chemicals (Indonesia).

Gelation time measurement. Gelation time was evaluated to determine the duration required for the composite hydrogel to transition into a non-flowable gel state. Samples were prepared in cylindrical molds with dimensions approximating 10 mm in diameter and 5 mm in height, mimicking the size of a native nucleus pulposus. The surface gelation time (when the top layer no longer flows upon tilting) and full-body gelation time (when the entire sample solidifies uniformly) were recorded using a stopwatch under ambient room temperature (~25 °C) through visual observation. This assessment was essential for validating the applicability of the hydrogel for injectable systems. Previous studies report that alginate-based hydrogels exhibit gelation times between 5–30 minutes, suitable for biomedical applications such as tissue engineering and wound healing.[19,31–33]

Fourier transform infrared spectroscopy (FTIR). To characterize the chemical structure of the hydrogel, FTIR spectra were acquired using a Thermo Scientific Nicolet IS10 instrument over a wavenumber range of 400–4000 cm^{-1}, with a resolution of 4 cm^{-1} and 32 scans per sample. The purpose of the analysis was to identify characteristic functional groups such as hydroxyl (O–H), carbonyl (C=O), and ether (C–O–C) bonds associated with PVA and alginate components.

Scanning electron microscopy (SEM) and energy-dispersive X-ray spectroscopy (EDS). Freeze-dried hydrogel specimens were prepared in cube-shaped samples measuring 1 cm × 1 cm × 1 cm, sputter-coated with platinum for 90 seconds at 20 mA to produce a ~10 nm coating. The specimens were then analyzed using a FEI INSPECT S50 operating at 15 kV, equipped with an EDS system. SEM imaging was performed to observe surface morphology and porosity, while EDS analysis was used to detect the spatial distribution of key elements, particularly Ba (from $BaSO_4$), Na (from Na_2HPO_4), and S (from $CaSO_4$), to confirm the homogeneity and integration of inorganic fillers in the hydrogel matrix.

Radiopacity testing. X-ray imaging was performed using a Shimadzu X-200 radiography unit at 60 kV and 5 mA on disc-shaped hydrogel samples with a diameter of 10 mm and a thickness of 2.5 mm. Radiographic images were analyzed using Adobe Photoshop (Histogram Tool) to evaluate radiopacity by measuring the mean grayscale brightness values on a 0–255 scale, where higher values indicated greater radiopacity. For consistency, each sample was measured in triplicate using a fixed Region of Interest (ROI) to minimize background variation.

Compressive strength testing. The compressive strength of the hydrogel samples was evaluated using a Universal Testing Machine (Hung TA Model HT-2402 series 4035) with a crosshead speed of 1 mm min^{-1}. The specimens were cylindrical in shape, with a diameter of 10 mm and a height of 20 mm. Testing was performed at room temperature, and values were averaged over three replicates to ensure reliability.

MTT assay for biocompatibility evaluation. The *in vitro* biocompatibility of the hydrogel was assessed using the MTT assay. Osteoblast-like 7F2 mouse cells (ATCC® CRL-12557™) were cultured in 96-well plates at a density of 1 × 10^4 cells per well for 24 hours, followed by treatment with hydrogel samples at a concentration of 10 mg per mL per well. After removal of the culture medium, cells were incubated with MTT solution (0.5 mg mL^{-1} in DMEM) for 4 hours at 37 °C. The resulting formazan crystals were dissolved in dimethyl sulfoxide (DMSO), and absorbance was measured at 570 nm using a Bio-Rad

iMark™ microplate reader. Cell viability was calculated by comparing absorbance values of treated samples with those of the untreated control group, where higher absorbance indicated greater viability.

Swelling and biodegradation tests. To assess the hydrogel's swelling behavior and biodegradability, samples were first freeze-dried using standard lyophilization techniques at −50 °C for 24 hours. The dry weights of the specimens were recorded, and the samples were immersed in phosphate-buffered saline (PBS, pH 7.4) at 37 °C to simulate physiological conditions.[34] At predetermined time intervals (1, 3, and 5 hours), the hydrogels were removed, gently blotted using filter paper to remove excess surface water, and weighed. The swelling ratio (Q) was calculated as:

$$Q = (W_S - W_0)/W_0 \quad (1)$$

where W_S is the weight of the swollen hydrogel at time t, and W_0 is the initial weight of the dry hydrogel.[35]

For biodegradation analysis, swollen samples were incubated in PBS at 37 °C over the same time intervals (1, 3, and 5 hours). After each time point, samples were dried under vacuum and reweighed to determine the percentage of weight loss, indicating hydrogel degradation.[36] These evaluations provide insights into the hydrogel's environmental responsiveness, drug delivery potential, and biodegradability under physiological conditions.[37]

Results and discussion

Gelation time analysis

Gelation time measurements were performed after pouring the synthesized hydrogel into nucleus pulposus molds. The data presented in Fig. 1 indicate that the sample with 1 wt% $BaSO_4$ and 0.3 wt% Na_2HPO_4 achieved the shortest gelation time, with the 70 : 30 ALG/PVA ratio yielding 9.0 ± 1.0 minutes and the 80 : 20 ratio showing 8.5 ± 1.5 minutes. Conversely, the longest gelation times were observed in samples with 1.5 wt% $BaSO_4$ and 0.5 wt% Na_2HPO_4. This trend demonstrates that gelation time increases with higher Na_2HPO_4 concentrations, likely due to the phosphate group's ability to compete with calcium ions, thereby retarding the ionic crosslinking between alginate and $CaSO_4$ (Table 1).[20]

Interestingly, the expectation that higher Ba^{2+} concentrations from $BaSO_4$ would accelerate gelation was not met, likely due to a synergistic interaction with Na_2HPO_4. While Ba^{2+} ions can act as secondary crosslinkers, the presence of Na_2HPO_4 is believed to disrupt Ca^{2+}-mediated gelation and reduce Ca^{2+} ion accessibility, possibly due to increased hydrogel matrix densification. This dual mechanism results in prolonged gelation

Table 1 The effect of addition Na_2HPO_4 and $BaSO_4$ in gelation time of hydrogel composite ALG/PVA/$BaSO_4$

	Gelation time (minutes)	
	Criteria 5–30 minutes[37]	
Sample	70 : 30	80 : 20
Na_2HPO_4 0.5%	14.0 ± 1.0	12.0 ± 1.0
$BaSO_4$ 1%/Na_2HPO_4 0.3%	09.0 ± 1.0	08.5 ± 1.5
$BaSO_4$ 1%/Na_2HPO_4 0.4%	12.5 ± 0.5	10.0 ± 2.0
$BaSO_4$ 1%/Na_2HPO_4 0.5%	15.0 ± 1.0	12.5 ± 1.5
$BaSO_4$ 1.5%/Na_2HPO_4 0.3%	11.5 ± 1.5	10.0 ± 1.0
$BaSO_4$ 1.5%/Na_2HPO_4 0.4%	12.5 ± 0.5	11.5 ± 1.5
$BaSO_4$ 1.5%/Na_2HPO_4 0.5%	15.5 ± 0.5	12.5 ± 1.5
Na_2HPO_4 0.5%	14.0 ± 1.0	12.0 ± 1.0
$BaSO_4$ 1%/Na_2HPO_4 0.3%	09.0 ± 1.0	08.5 ± 1.5
$BaSO_4$ 1%/Na_2HPO_4 0.4%	12.5 ± 0.5	10.0 ± 2.0
$BaSO_4$ 1%/Na_2HPO_4 0.5%	15.0 ± 1.0	12.5 ± 1.5
$BaSO_4$ 1.5%/Na_2HPO_4 0.3%	11.5 ± 1.5	10.0 ± 1.0
$BaSO_4$ 1.5%/Na_2HPO_4 0.4%	12.5 ± 0.5	11.5 ± 1.5
$BaSO_4$ 1.5%/Na_2HPO_4 0.5%	15.5 ± 0.5	12.5 ± 1.5

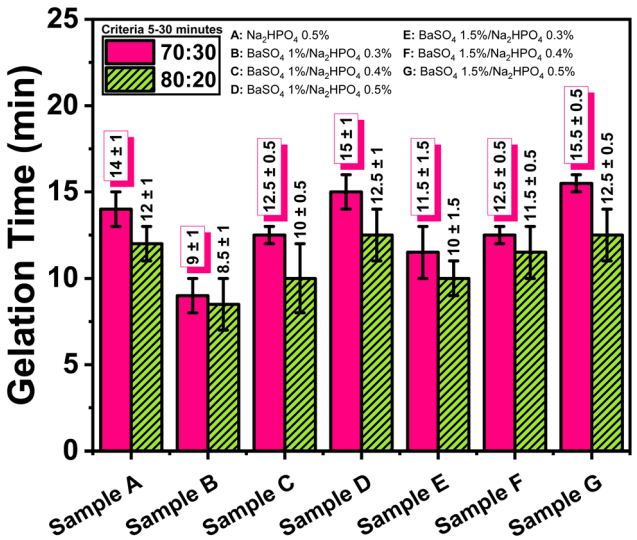

Fig. 1 Effect of Na_2HPO_4 and $BaSO_4$ addition on the gelation time of ALG/PVA/$BaSO_4$ hydrogel composites.

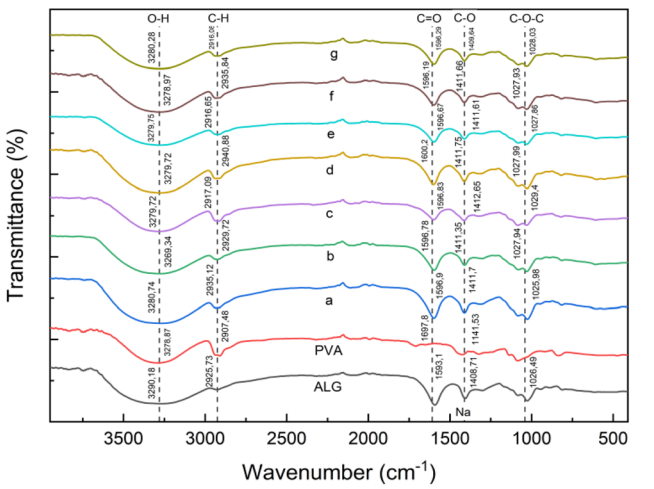

Fig. 2 FTIR spectra of ALG/PVA/$BaSO_4$ (70 : 30) hydrogels with varying Na_2HPO_4 and $BaSO_4$ content: (a) Na_2HPO_4, 0.5%; (b) $BaSO_4$ 1%, Na_2HPO_4 0.3%; (c) $BaSO_4$ 1%, Na_2HPO_4 0.4%; (d) $BaSO_4$ 1%, Na_2HPO_4 0.5%; (e) $BaSO_4$ 1.5%, Na_2HPO_4 0.3%; (f) $BaSO_4$ 1.5%, Na_2HPO_4 0.4%; (g) $BaSO_4$ 1.5%, Na_2HPO_4 0.5%.

time, aligning with prior observations on $BaSO_4$'s role in alginate-based hydrogels.[20,38] Nonetheless, all hydrogel formulations exhibited gelation times within the clinically acceptable range of 5–30 minutes, which is crucial for maintaining injectability and handling during *in situ* application.[39]

FTIR analysis

FTIR analysis of the 70 : 30 and 80 : 20 ALG/PVA/$BaSO_4$ hydrogels revealed characteristic peaks associated with PVA and alginate functional groups (Fig. 2 and 3). For PVA peaks were identified at 2907 cm^{-1} (O–H), 1697 cm^{-1} (C=O), and 1141 cm^{-1} (C–O). Alginate displayed absorption at 3290 cm^{-1}, 2925 cm^{-1}, 1593 cm^{-1}, 1408 cm^{-1}, and 1026 cm^{-1} consistent with O–H, C–H, C=O, C–O–Na, and C–O–C groups respectively. The shift

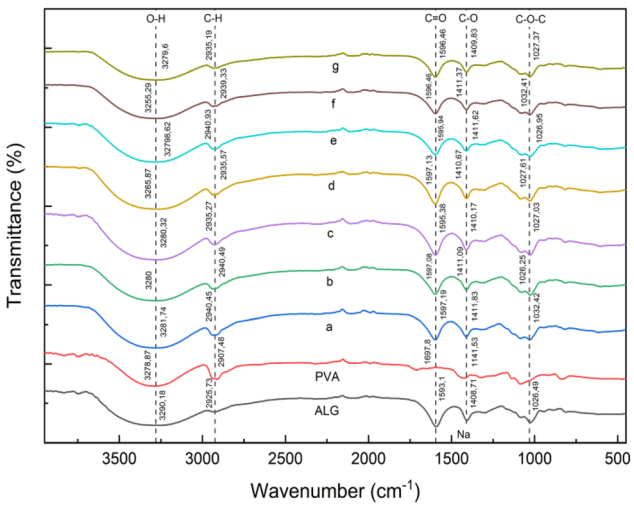

Fig. 3 FTIR spectra of ALG/PVA/$BaSO_4$ (80 : 20) hydrogels with varying Na_2HPO_4 and $BaSO_4$ content: (a) Na_2HPO_4, 0.5%; (b) $BaSO_4$ 1%, Na_2HPO_4 0.3%; (c) $BaSO_4$ 1%, Na_2HPO_4 0.4%; (d) $BaSO_4$ 1%, Na_2HPO_4 0.5%; (e) $BaSO_4$ 1.5%, Na_2HPO_4 0.3%; (f) $BaSO_4$ 1.5%, Na_2HPO_4 0.4%; (g) $BaSO_4$ 1.5%, Na_2HPO_4 0.5%.

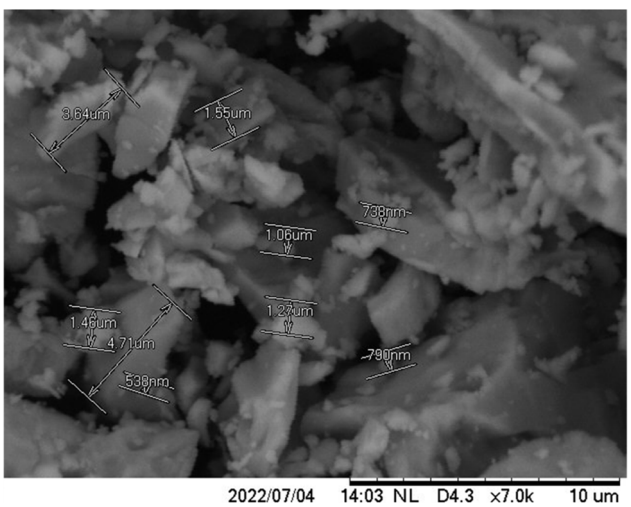

Fig. 4 SEM image of $BaSO_4$ particles.

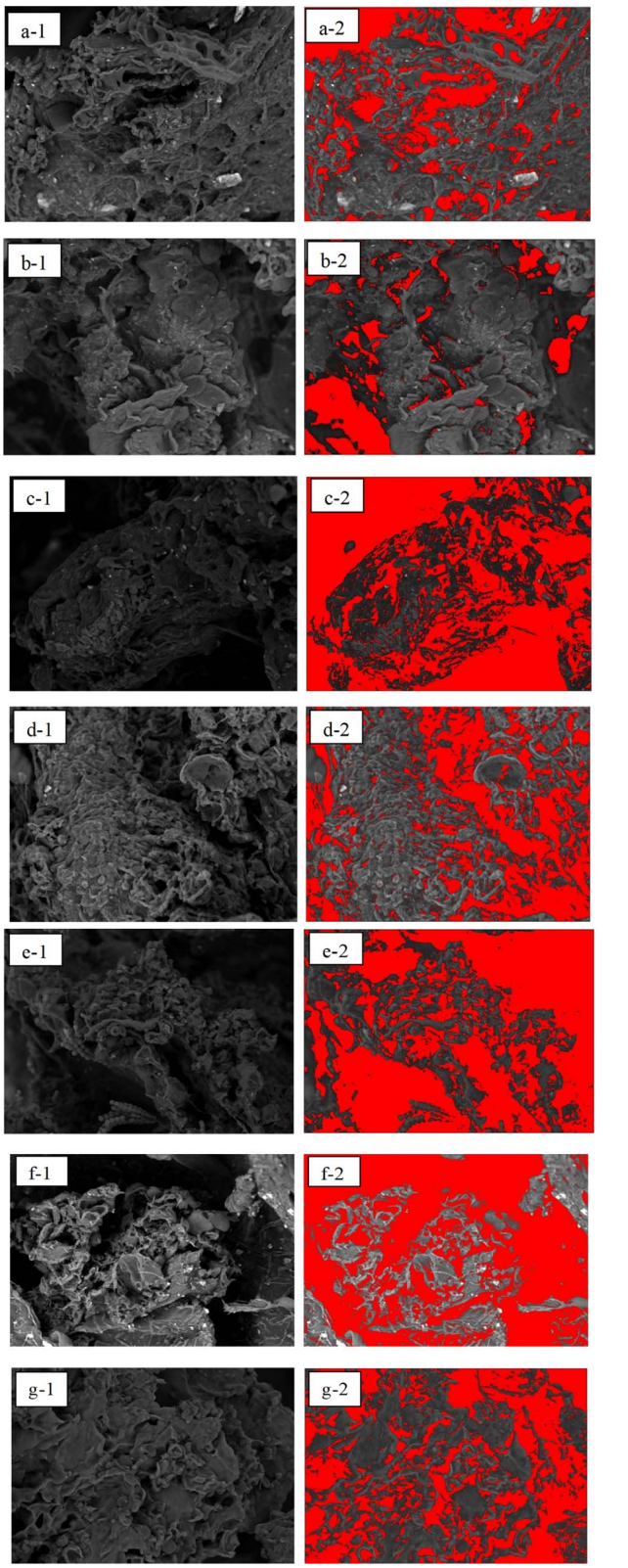

Fig. 5 (1) SEM test results for the ALG/PVA/$BaSO_4$ hydrogel variation 70 : 30 at 1.000× magnification; (a) $BaSO_4$ 1%/Na_2HPO_4 0.3%. (b) $BaSO_4$ 1%/Na_2HPO_4 0.4%. (c) $BaSO_4$ 1%/Na_2HPO_4 0.5%. (d) $BaSO_4$ 1.5%/Na_2HPO_4 0.3%. (e) $BaSO_4$ 1.5%/Na_2HPO_4 0.4%. (f) $BaSO_4$ 1.5%/Na_2HPO_4 0.5%. (g) Na_2HPO_4 0.5%; (2) the results of pore identification using ImageJ software.

observed in the hydroxyl band suggests intermolecular hydrogen bonding between the alginate and PVA chains, indicating successful polymer interaction during hydrogel formation.[40]

Morphological analysis (SEM and EDS)

SEM analysis of $BaSO_4$ (Fig. 4) showed particle sizes ranging from 538 nm to 4.71 μm with irregular crystalline morphology, which aligns with previously reported characteristics. Before analyzing the composite hydrogels, $BaSO_4$ morphology was examined to understand its integration behavior within the matrix. SEM imaging of the 70 : 30 ALG/PVA/$BaSO_4$ hydrogel at 1000× magnification (Fig. 5) revealed heterogeneous pore structures. The porosity was quantified using ImageJ software (Fig. 6, Tables 2 and 3). The highest porosity (85.89%) was observed in the sample containing 1.5 wt% $BaSO_4$ and 0.4 wt% Na_2HPO_4, closely approaching the reported scaffold suitability threshold of 81.28 ± 4.10%.[41]

Pore sizes between 100–400 μm are optimal for cell attachment and proliferation. Most hydrogel variants met this criterion. However, two specific formulations—those without $BaSO_4$ and those containing 1.5 wt% $BaSO_4$ with 0.5 wt% Na_2HPO_4—exhibited smaller pore sizes that fell below this optimal range (Table 2).

EDS mapping (Fig. 7) confirmed the spatial distributions of Ba, Na, and S, represented by blue, green, and red signals, respectively. However, the observed agglomeration of $BaSO_4$ particles reduced their dispersion efficiency within the matrix, which may hinder uniform mechanical reinforcement and cell interaction. This suggests that further interfacial modification could improve matrix-particle bonding and nucleation uniformity.[42]

Radiopacity evaluation

Radiopacity evaluation was conducted to determine the X-ray visibility of the hydrogels, which is critical for biomedical imaging applications. X-ray imaging (Fig. 8) was used to assess image brightness (radiopacity), which increased with $BaSO_4$ concentration, consistent with previous studies.[43] The 1.5 wt% $BaSO_4$ sample displayed the highest radiopacity. Furthermore, Hue–Saturation–Brightness (HSB) analysis (Table 4) confirmed this trend, with 76% brightness measured for the 80 : 20 hydrogel ratio.

Table 2 Percent porosity of ALG/PVA/$BaSO_4$ hydrogel composites

	% porosity	
	81.28 ± 4.10%	
Sample	70 : 30	80 : 20
Na_2HPO_4 0.5%	23	18.99
$BaSO_4$ 1%/Na_2HPO_4 0.3%	40.58	41.66
$BaSO_4$ 1%/Na_2HPO_4 0.4%	75.85	79.38
$BaSO_4$ 1%/Na_2HPO_4 (0.5%)	28.07	24.41
$BaSO_4$ 1.5%/Na_2HPO_4 0.3%	60	68.24
$BaSO_4$ 1.5%/Na_2HPO_4 0.4%	83.125	85.89
$BaSO_4$ 1.5%/Na_2HPO_4 0.5%	37.51	31.19

Table 3 Pore size of the ALG/PVA/$BaSO_4$ hydrogel composites

	Pore size (μm)	
	100–400 μm	
Sample	70 : 30	80 : 20
Na_2HPO_4 0.5%	84	87.32
$BaSO_4$ 1%/Na_2HPO_4 0.3%	101.41	110.63
$BaSO_4$ 1%/Na_2HPO_4 0.4%	117.28	118.6
$BaSO_4$ 1%/Na_2HPO_4 (0.5%)	92.47	92.65
$BaSO_4$ 1.5%/Na_2HPO_4 0.3%	110.63	110.78
$BaSO_4$ 1.5%/Na_2HPO_4 0.4%	120.07	122.8
$BaSO_4$ 1.5%/Na_2HPO_4 0.5%	95.75	96.18

Mechanical characterization

Young's modulus values (Table 5) of all hydrogel composites ranged from 0.020 to 0.090 MPa, which is within the range of native nucleus pulposus (NP) tissue modulus (0.0649 ± 0.044

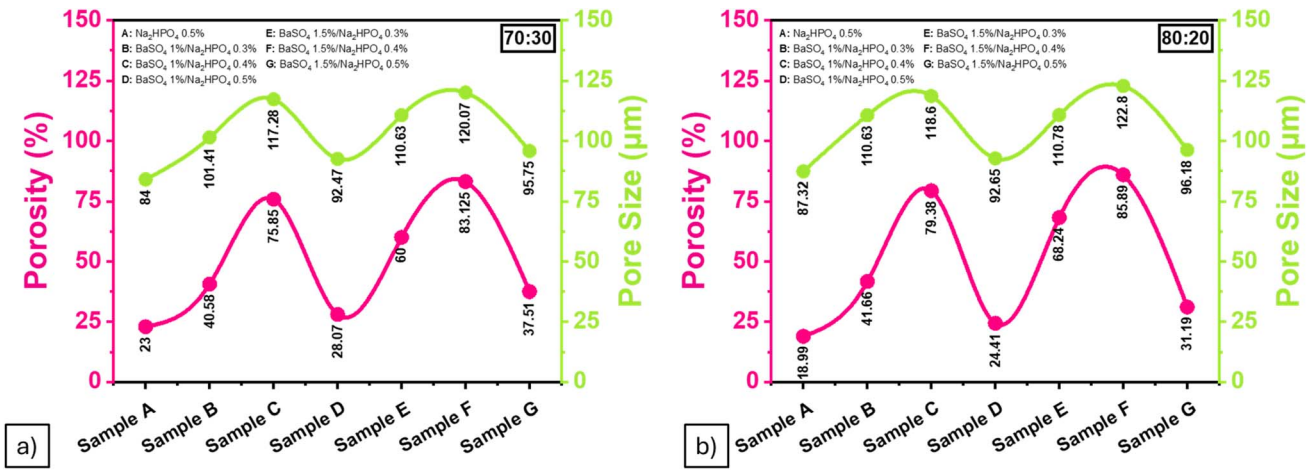

Fig. 6 Percent porosity and pore size of ALG/PVA/$BaSO_4$ hydrogel composites from (a) 70 : 30, (b) 80 : 20 ratio.

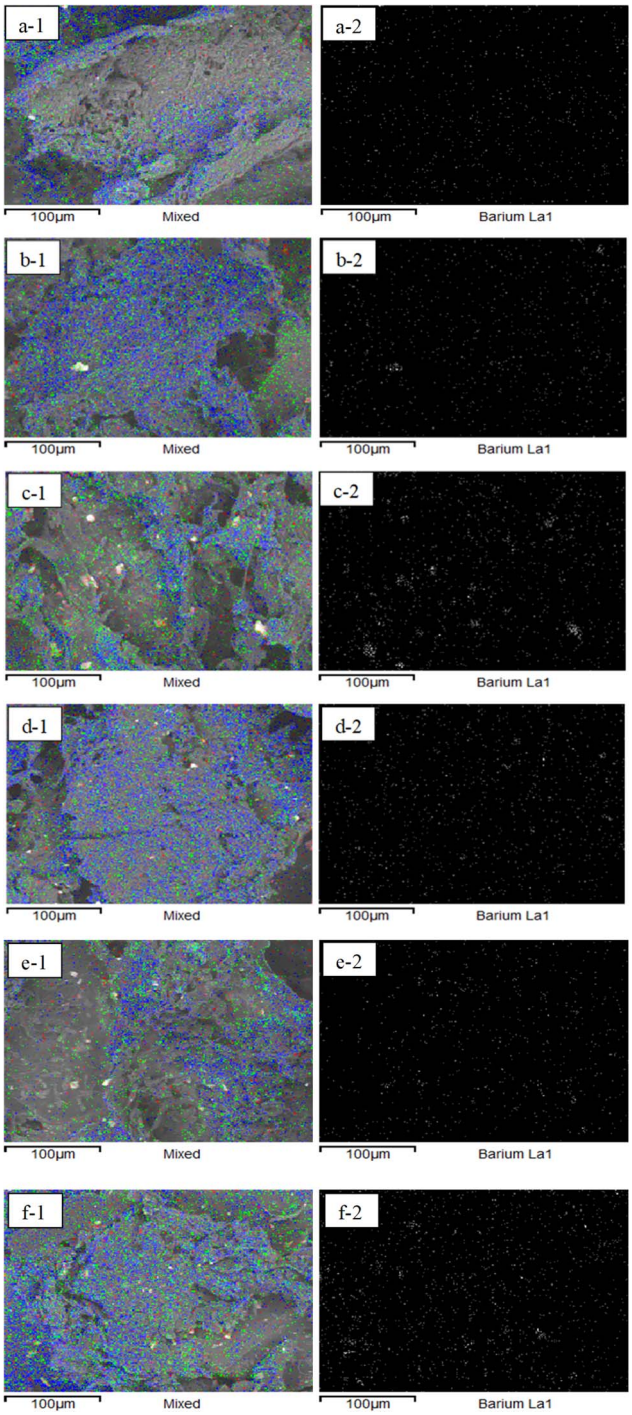

Fig. 7 (1) Mapping of elements on ALG/PVA/$BaSO_4$ hydrogel variation 70 : 30 [blue is barium, green is sodium, and red is sulfur]; (a) $BaSO_4$ 1%/Na_2HPO_4 0.3%, (b) $BaSO_4$ 1%/Na_2HPO_4 0.4%, (c) $BaSO_4$ 1%/Na_2HPO_4 0.5%, (d) $BaSO_4$ 1.5%/Na_2HPO_4 0.3%, (e) $BaSO_4$ 1.5%/Na_2HPO_4 0.4%, (f) $BaSO_4$ 1.5%/Na_2HPO_4 0.5%; (2) mapping the distribution of barium ALG/PVA/$BaSO_4$ hydrogel.

MPa). Notably, the formulation containing 1.5 wt% $BaSO_4$ and 0.4 wt% Na_2HPO_4 exhibited the highest modulus (0.090 ± 0.040 MPa), which closely matches the upper bound of the NP modulus range (Fig. 9).

However, the compressive strength values (Table 6 and Fig. 10) fell short of the mechanical requirements for NP, which range from 0.091 to 1.33 MPa under physiological loading.[45] Although higher porosity typically weakens mechanical integrity, formulations containing 1.5 wt% $BaSO_4$, particularly in the 70 : 30 ratio with 0.4 wt% Na_2HPO_4, showed comparatively improved strength. This enhancement may result from better $BaSO_4$ particle packing and scaffold densification; however, the values remain below the physiological threshold, indicating the need for further mechanical optimization.

Despite the compressive strengths remaining below NP-relevant levels, the data highlight a complex relationship among porosity, composition, and mechanical behavior. Reinforcement strategies such as nanofibers or hybrid scaffolds are needed for future improvement. These findings suggest a necessary trade-off between achieving optimal porosity for biological integration and sufficient mechanical robustness, which should be carefully balanced in future scaffold designs.

Biocompatibility assessment

MTT assay results (Table 7 and Fig. 11) demonstrate that most hydrogel formulations achieved high cell viability exceeding 90%, especially those containing 1% $BaSO_4$ and 0.5% Na_2HPO_4 in both 70 : 30 and 80 : 20 ALG/PVA ratios. In contrast, formulations with 1.5% $BaSO_4$ and 0.4% Na_2HPO_4 exhibited significantly reduced viability (~79%), suggesting a possible concentration-dependent cytotoxic response. Several combinations, such as 1% $BaSO_4$ with 0.3% Na_2HPO_4 and 1.5% $BaSO_4$ with 0.5% Na_2HPO_4 in the 70 : 30 ratio, resulted in non-detectable or inconsistent viability data (N/A), potentially due to poor dispersion or localized accumulation of $BaSO_4$ particles, which has been associated with cytotoxic effects.[47,48] Despite these anomalies, the overall data support the biocompatibility of the composite, particularly in optimized concentrations that balance radiopacity with cellular health. Among the tested polymer ratios, the 80 : 20 composition generally yielded slightly higher cell viability values, indicating improved compatibility at lower PVA content.

The two-way ANOVA results (Table 8) indicate that both the sample composition ($p < 0.001$) and the ALG/PVA polymer ratio ($p = 0.003$) exert statistically significant effects on cell viability outcomes. Moreover, a significant interaction was observed between sample composition and polymer ratio ($F = 5.933$, $p = 0.003$), suggesting that the effect of composition on viability is dependent on the specific polymer blend used. The model yielded a high coefficient of determination (adjusted $R^2 = 0.906$), indicating that over 90% of the variance in cell viability can be explained by these two variables and their interaction. These findings reinforce the importance of fine-tuning both $BaSO_4$/Na_2HPO_4 concentrations and the polymer blend ratio to maximize biocompatibility in hydrogel scaffold design.

Swelling behavior

The swelling behavior of the hydrogels demonstrated a significant time-dependent increase in water uptake, with swelling ratios ranging from approximately 400% to 800% over a 5-hour

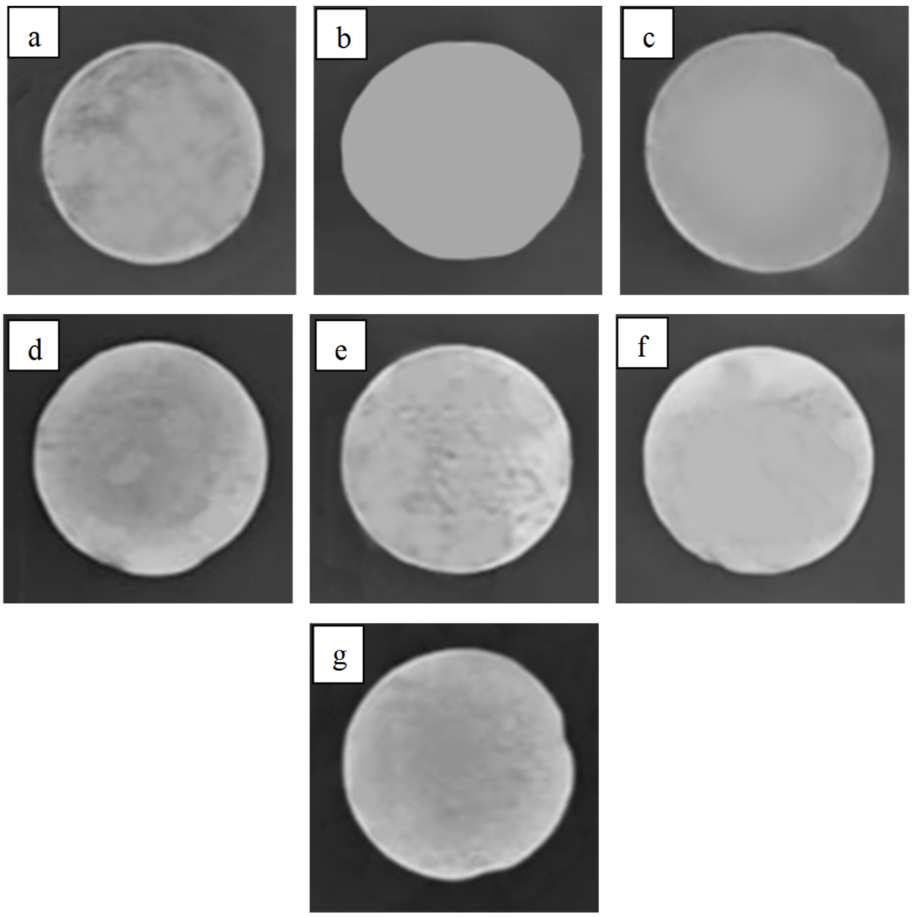

Fig. 8 Results of radiopacity testing on ALG/PVA/$BaSO_4$ hydrogel variation 70 : 30; (a) Na_2HPO_4 0.5%, (b) $BaSO_4$ 1%/Na_2HPO_4 0.3%, (c) $BaSO_4$ 1%/Na_2HPO_4 0.4%, (d) $BaSO_4$ 1%/Na_2HPO_4 0.5%, (e) $BaSO_4$ 1.5%/Na_2HPO_4 0.3%, (f) $BaSO_4$ 1.5%/Na_2HPO_4 0.4%, (g) $BaSO_4$ 1.5%/Na_2HPO_4 0.5%.

Table 4 The brightness of radiopacity results

	% brightness	
Sample	70 : 30	80 : 20
Na_2HPO_4 0.5%	65	66
$BaSO_4$ 1%/Na_2HPO_4 0.3%	66	68
$BaSO_4$ 1%/Na_2HPO_4 0.4%	69	70
$BaSO_4$ 1%/Na_2HPO_4 0.5%	70	71
$BaSO_4$ 1.5%/Na_2HPO_4 0.3%	71	73
$BaSO_4$ 1.5%/Na_2HPO_4 0.4%	71	74
$BaSO_4$ 1.5%/Na_2HPO_4 0.5%	73	76

Table 5 Young modulus values of the ALG/PVA/$BaSO_4$ hydrogel composites

	Young modulus (MPa)	
	0.0649 ± 0.044 MPa (ref. 44)	
Sample	70 : 30	80 : 20
Na_2HPO_4 0.5%	0.055 ± 0.005	0.055 ± 0.005
$BaSO_4$ 1%/Na_2HPO_4 0.3%	0.030 ± 0.000	0.045 ± 0.015
$BaSO_4$ 1%/Na_2HPO_4 0.4%	0.025 ± 0.005	0.025 ± 0.005
$BaSO_4$ 1%/Na_2HPO_4 0.5%	0.060 ± 0.010	0.060 ± 0.000
$BaSO_4$ 1.5%/Na_2HPO_4 0.3%	0.030 ± 0.000	0.020 ± 0.000
$BaSO_4$ 1.5%/Na_2HPO_4 0.4%	0.090 ± 0.040	0.055 ± 0.015
$BaSO_4$ 1.5%/Na_2HPO_4 0.5%	0.035 ± 0.005	0.030 ± 0.000

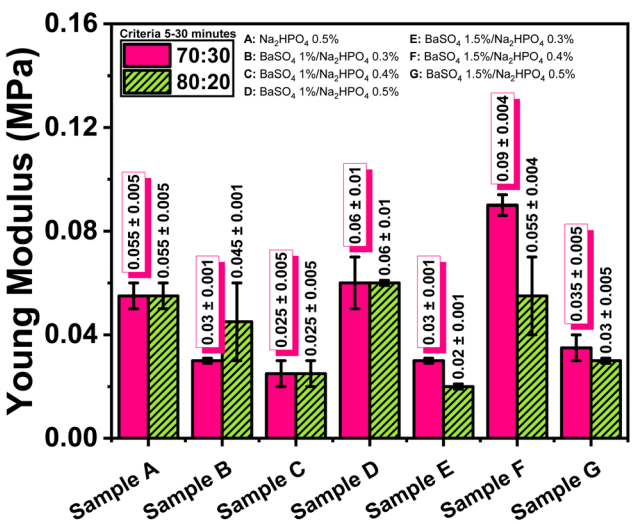

Fig. 9 Young modulus values of the ALG/PVA/$BaSO_4$ hydrogel composites.

immersion period. This substantial increase indicates efficient fluid absorption capacity, a key feature of hydrogels intended for biomedical applications. Maintaining high levels of hydration is critical in nucleus pulposus (NP) regeneration,[49] as it

Table 6 Compressive strength values of the ALG/PVA/$BaSO_4$ hydrogel composite (ap, b, and N refer to alginate/PVA 70 : 30, $BaSO_4$, and Na_2HPO_4 respectively. The capital letters represent the variation 80 : 20)

	Compressive strength in some conditions for intervertebral disc (MPa)[46]			
Sample	Sitting (0.46–1.330 Mpa)	Standing (0.5–0.87 Mpa)	Lying (0.091–0.539 Mpa)	Carrying 20 kg of load (2.3 Mpa)
apn0.5	0.015 ± 0.002	0.015 ± 0.002	0.015 ± 0.002	0.015 ± 0.002
apb1n0.3	0.006 ± 0.001	0.006 ± 0.001	0.006 ± 0.001	0.006 ± 0.001
apb1n0.4	0.007 ± 0.000	0.007 ± 0.000	0.007 ± 0.000	0.007 ± 0.000
apb1n0.5	0.011 ± 0.001	0.011 ± 0.001	0.011 ± 0.001	0.011 ± 0.001
apb1.5n0.3	0.008 ± 0.000	0.008 ± 0.000	0.008 ± 0.000	0.008 ± 0.000
apb1.5n0.4	0.024 ± 0.012	0.024 ± 0.012	0.024 ± 0.012	0.024 ± 0.012
ap1.5n0.5	0.007 ± 0.001	0.007 ± 0.001	0.007 ± 0.001	0.007 ± 0.001
APN0.5	0.013 ± 0.000	0.013 ± 0.000	0.013 ± 0.000	0.013 ± 0.000
APB1N0.3	0.011 ± 0.002	0.011 ± 0.002	0.011 ± 0.002	0.011 ± 0.002
APB1N0.4	0.005 ± 0.001	0.005 ± 0.001	0.005 ± 0.001	0.005 ± 0.001
APB1N0.5	0.011 ± 0.000	0.011 ± 0.000	0.011 ± 0.000	0.011 ± 0.000
APB1.5N0.3	0.006 ± 0.001	0.006 ± 0.001	0.006 ± 0.001	0.006 ± 0.001
APB1.5N0.4	0.013 ± 0.003	0.013 ± 0.003	0.013 ± 0.003	0.013 ± 0.003
APB1.5N0.5	0.006 ± 0.000	0.006 ± 0.000	0.006 ± 0.000	0.006 ± 0.000

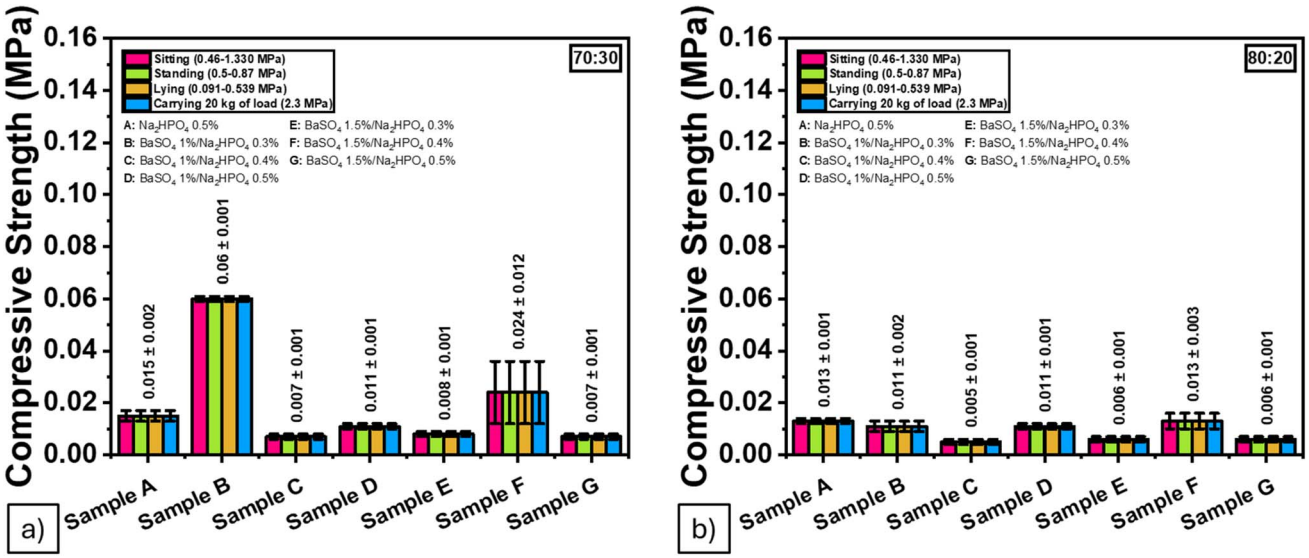

Fig. 10 Compressive strength values of the ALG/PVA/$BaSO_4$ hydrogel composite from (a) 70 : 30, (b) 80 : 20 ratio.

Table 7 Effect of $BaSO_4$ and Na_2HPO_4 on cell viability of the ALG/PVA hydrogel composite

	Cell viability (%)	
Sample	70 : 30	80 : 20
Control positive	100	
Control negative	0	
Na_2HPO_4 0.5%	89.576 ± 1.11	83.576 ± 3.12
$BaSO_4$ 1%/Na_2HPO_4 0.3%	N/A	N/A
$BaSO_4$ 1%/Na_2HPO_4 0.4%	91.634 ± 0.48	89.269 ± 1.88
$BaSO_4$ 1%/Na_2HPO_4 0.5%	90.155 ± 0.98	91.064 ± 0.98
$BaSO_4$ 1.5%/Na_2HPO_4 0.3%	N/A	96.139 ± 0.43
$BaSO_4$ 1.5%/Na_2HPO_4 0.4%	79.529 ± 0.829	79.137 ± 0.132
$BaSO_4$ 1.5%/Na_2HPO_4 0.5%	N/A	92.350 ± 1.526

helps preserve disc height and mechanical function under compressive loads. Therefore, the observed swelling performance reinforces the potential applicability of ALG/PVA/$BaSO_4$ composites for intervertebral disc repair. This trend is illustrated in Fig. 12.

Short-term degradation

These short-term results are consistent with previous studies reporting rapid water uptake in superabsorbent hydrogels.[50,51] While this experiment did not assess long-term biodegradation, the observed early-stage degradation behavior offers meaningful insights into hydrogel stability and assists in identifying

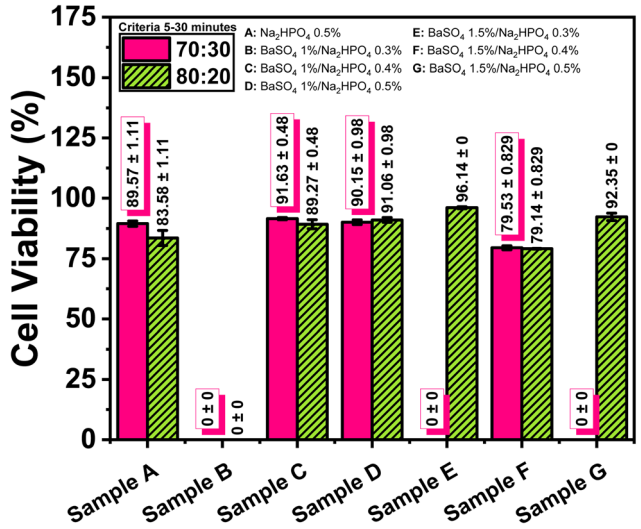

Fig. 11 Effect of $BaSO_4$ and Na_2HPO_4 on cell viability of the ALG/PVA hydrogel composite.

Table 9 Initial degradation behavior of ALG/PVA/$BaSO_4$ hydrogel composites over 5 hours (short-term assessment)

	Degradation rate (%)		
Duration	$BaSO_4$ 1%/Na_2HPO_4 0.4%	$BaSO_4$, 1.5%; Na_2HPO_4, 0.4%	$CaSO_4$ 1%
70 : 30			
1 hour	10.84 ± 3.4	17.58 ± 11.3	18.08 ± 8.5
3 hour	24.36 ± 12.3	30.12 ± 19.8	31.57 ± 12.4
5 hour	37.27 ± 14.2	22.96 ± 14.9	41.80 ± 11.2
80 : 20			
1 hour	6.05 ± 0.6	5.28 ± 8.9	12.88 ± 2.6
3 hour	−0.18 ± 6.06	26.40 ± 16.3	19.32 ± 3.4
5 hour	7.52 ± 5.51	8.01 ± 9.2	28.84 ± 5.5

suitable formulations for future durability studies (Table 9 and Fig. 13).

The overarching objective of this study was to develop an injectable, biocompatible, and radiopaque hydrogel composite suitable for nucleus pulposus (NP) regeneration. Each of the experimental findings—gelation time, structural analysis, mechanical performance, swelling behavior, degradation rate, and cytocompatibility—collectively supports the feasibility of this formulation for clinical application. Optimized concentrations of Na_2HPO_4 and $BaSO_4$ yielded short gelation times (8.5–15.5 min), which fall within the recommended range for *in situ* injectability during minimally invasive spinal procedures (5–30 minutes). FTIR results demonstrated that the crosslinking process is dominated by physical interactions, as evidenced by unaltered characteristic peaks of alginate and PVA, thereby

Table 8 Two-way analysis of effect of $BaSO_4$ and Na_2HPO_4 on cell viability of the ALG/PVA hydrogel composite[a]

Source	Type III sum of squares	df	Mean square	F	Sig
Corrected model	1138.889	9	126.543	42.925	0.000
Intercept	295 139.141	1	295 139.141	100 114.007	0.000
Sample_Comp	1078.890	5	215.778	73.194	0.000
Ratio	29.884	1	29.884	10.137	0.003
Sample_Comp*Ratio	52.475	3	17.492	5.933	0.003
Error	88.441	30	2.948		
Total	312 784.601	40			
Corrected total	1227.330	39			

[a] R squared = 0.928 (adjusted R squared = 0.906).

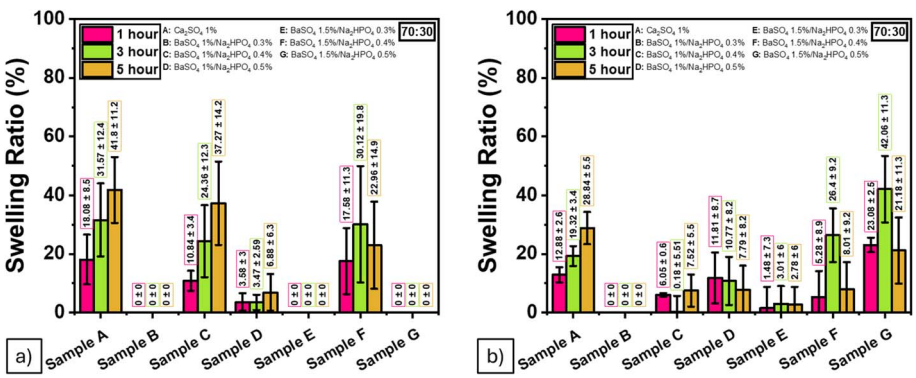

Fig. 12 Swelling ratios of the ALG/PVA/$BaSO_4$ hydrogel composites at different time points from (a) 70 : 30, (b) 80 : 20 ratio.

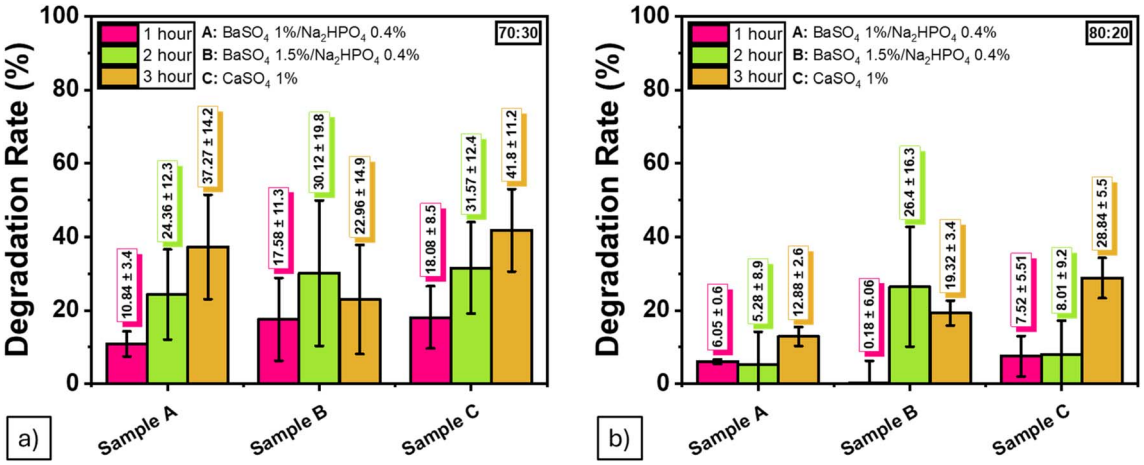

Fig. 13 Initial degradation behavior of ALG/PVA/$BaSO_4$ hydrogel composites over 5 hours from (a) 70 : 30, (b) 80 : 20 ratio (short-term assessment).

preserving the chemical stability of the base polymers and confirming the bioinert nature of $BaSO_4$.

Morphological observations revealed that hydrogels containing 1.5 wt% $BaSO_4$ and 0.4 wt% Na_2HPO_4 exhibited the highest porosity and pore sizes, which are considered favorable for biomedical scaffolds. Such microstructures facilitate cell infiltration and nutrient diffusion, essential for tissue integration and long-term scaffold performance.[41] SEM and EDS analysis also revealed $BaSO_4$ agglomeration in some samples, suggesting the need for improved interfacial compatibility between filler particles and the polymer matrix to ensure consistent dispersion and mechanical uniformity.

Radiopacity increased in direct proportion to $BaSO_4$ content, enabling clear X-ray visualization of the hydrogel implants—a critical requirement for monitoring implant placement and integrity during spinal procedures. Mechanical analysis showed that while the elastic modulus of several formulations (ranging from 0.025 to 0.090 MPa) fell within the acceptable range for native NP tissue (0.0649 ± 0.044 MPa), the compressive strengths remained well below physiological benchmarks (0.091–1.33 MPa). This mismatch highlights the need for future reinforcement strategies—such as incorporating reinforcing nanofillers or developing dual-network systems—to improve the hydrogel's load-bearing capacity.

Biocompatibility assessments revealed that formulations containing 1 wt% $BaSO_4$ and either 0.4% or 0.5% Na_2HPO_4 maintained high cell viability above 90%, indicating favorable cytocompatibility. However, formulations with 1.5 wt% $BaSO_4$—especially at 0.4% Na_2HPO_4—exhibited reduced viability (~79%), suggesting potential cytotoxic effects at higher $BaSO_4$ concentrations. Swelling and degradation analyses confirmed the hydrogel's strong water absorption and gradual mass loss under simulated physiological conditions, both of which are essential for maintaining hydration and replicating the functional environment of the native nucleus pulposus.

Overall, the results highlight a complex but consistent relationship between the hydrogel's chemical composition and its functional performance. Tuning the concentrations of $BaSO_4$ and Na_2HPO_4 not only improved gelation time and radiopacity but also influenced key parameters such as mechanical strength, porosity, and cytocompatibility. This interdependent behavior among formulation variables and performance metrics supports the hydrogel's potential as an injectable, biocompatible scaffold with radiopaque visibility for nucleus pulposus regeneration, while also emphasizing the need for further mechanical optimization.

Conclusion

This study aimed to evaluate the effects of varying concentrations of Na_2HPO_4 (0.3%, 0.4%, and 0.5%) and $BaSO_4$ (1% and 1.5%) on the physical, mechanical, and biological performance of ALG/PVA composite hydrogels as injectable scaffolds for nucleus pulposus (NP) regeneration. The optimal formulation—1.5 wt% $BaSO_4$ and 0.4 wt% Na_2HPO_4—demonstrated a gelation time of 12.5 ± 0.5 minutes, an elastic modulus of 0.055 ± 0.015 MPa, radiopacity of 71–74%, porosity above 80%, and cell viability exceeding 90%, thereby satisfying key criteria for NP applications. All hydrogel variations exhibited gelation times within the clinically acceptable range (5–30 minutes). The incorporation of $BaSO_4$ enhanced radiopacity in proportion to its concentration, while Na_2HPO_4 effectively modulated gelation kinetics.

Although elastic modulus values improved, the compressive strength (maximum 0.024 ± 0.012 MPa) remained below the physiological threshold (0.091–1.33 MPa), indicating a need for further mechanical enhancement. This study offers a promising foundation for the development of multifunctional hydrogels; however, future work should focus on improving mechanical load-bearing capacity through composite reinforcement and validating long-term *in vivo* performance.

In vitro biocompatibility tests using the MTT assay on osteoblast-like 7F2 cells showed that formulations with 0.4% and 0.5% Na_2HPO_4 achieved high cell viability (>90%), confirming favorable cytocompatibility. The formulation with 1%

$BaSO_4$ and 0.5% Na_2HPO_4 exhibited the highest viability (91.064 ± 0.98%). These results support the hydrogel's suitability for biomedical use, particularly in tissue engineering and regenerative medicine.

The swelling behavior showed a significant time-dependent increase in water absorption, supporting the hydrogel's ability to maintain hydration and structural integrity in the disc space. Additionally, degradation studies revealed that $CaSO_4$ decomposed faster than $BaSO_4$, emphasizing the importance of selecting appropriate radiopaque and retarding agents to tailor *in vivo* performance.

The dual incorporation of Na_2HPO_4 and $BaSO_4$ in a single system represents a novel approach that simultaneously addresses gelation kinetics and radiopacity requirements for injectable NP scaffolds.

In summary, while the hydrogel system shows strong potential in terms of biocompatibility, gelation behavior, and imaging visibility, future research must address mechanical reinforcement to fully meet clinical load-bearing demands.

Conflicts of interest

There are no conflicts to declare.

Data availability

Due to the confidential nature of the data, they are not publicly available. Data may be available from the corresponding author on reasonable request and subject to confidentiality agreements.

Acknowledgements

The authors gratefully acknowledge financial support from the Institut Teknologi Sepuluh Nopember under the project scheme of the Departmental Research Funding: Work Unit Fund Batch 2 – Institut Teknologi Sepuluh Nopember 2024, No. 2045/PKS/ITS/2024.

References

1 C. Yan, *et al.*, Applications of Functionalized Hydrogels in the Regeneration of the Intervertebral Disc, *BioMed Res. Int.*, 2021, **2021**(1), 2818624, DOI: 10.1155/2021/2818624.

2 C. Centeno, *et al.*, Treatment of lumbar degenerative disc disease-associated radicular pain with culture-expanded autologous mesenchymal stem cells: a pilot study on safety and efficacy, *J. Transl. Med.*, 2017, **15**(1), 197, DOI: 10.1186/s12967-017-1300-y.

3 L.-Y. Jin, *et al.*, Estradiol Alleviates Intervertebral Disc Degeneration through Modulating the Antioxidant Enzymes and Inhibiting Autophagy in the Model of Menopause Rats, *Oxid. Med. Cell. Longev.*, 2018, **2018**(1), 7890291, DOI: 10.1155/2018/7890291.

4 M. Ngwa and E. Agyingi, A mathematical model of the compression of a spinal disc, *Math. Biosci. Eng.*, 2011, **8**(4), 1061–1083, DOI: 10.3934/mbe.2011.8.1061.

5 A. Nachemson, Lumbar intradiscal pressure. Experimental studies on post-mortem material, *Acta Orthop. Scand. Suppl.*, 1960, **43**, 1–104, DOI: 10.3109/ort.1960.31.suppl-43.01.

6 Qi-B. Bao, G. M. Mccullen, P. A. Higham, J. H. Dumbleton and H. A. Yuan, The artificial disc: theory, design and materials, *Biomaterials*, 1996, **17**(Issue 12), 1157–1167, DOI: 10.1016/0142-9612(96)84936-2.

7 H. Suryandaru, A. A. N. Hanifah and A. Rasyida, Alginate/PVA/chitosan injection composites as scaffold material for nucleus pulposus regeneration, *IOP Conf. Ser. Earth Environ. Sci.*, 2021, **649**, 12019, DOI: 10.1088/1755-1315/649/1/012019.

8 J. Hu, *et al.*, Functional compressive mechanics and tissue biocompatibility of an injectable SF/PU hydrogel for nucleus pulposus replacement, *Sci. Rep.*, 2017, **7**(1), 2347, DOI: 10.1038/s41598-017-02497-3.

9 A. Rasyida, T. Rizkha Pradipta, S. Tri Wicaksono, V. Mitha Pratiwi and Y. Widya Rakhmawati, Preliminary Study of Alginates Extracted from Brown Algae (Sargassum sp.) Available in Madura Island as Composite Based Hydrogel Materials, *Mater. Sci. Forum*, 2019, **964**, 240–245.

10 A. Rasyida, Y. Silaen, T. Sigit, H. Ardyananta, H. Nurdiansah and S. Halimah, Preliminary Characterization of Hydrogel Composite Alginate/PVA/r-GO as an Injectable Materials for Medical Applications, *Mater. Sci. Forum*, 2019, **964**, 161–167, DOI: 10.4028/www.scientific.net/MSF.964.161.

11 M. Bahadoran, A. Shamloo and Y. D. Nokoorani, Development of a polyvinyl alcohol/sodium alginate hydrogel-based scaffold incorporating bFGF-encapsulated microspheres for accelerated wound healing, *Sci. Rep.*, 2020, **10**(1), 7342, DOI: 10.1038/s41598-020-64480-9.

12 G. I. Permana, A. H. Bajamal, E. A. Subagio, M. A. Parenrengi, A. Rasyida and B. Utomo, Novel Silicone Rubber and Polyvinyl Alcohol (PVA) Compound as Nucleus Pulposus Replacement in Intervertebral Disc Herniation Surgery, *Turk. Neurosurg.*, 2022, **32**(5), 779–785, DOI: 10.5137/1019-5149.JTN.35925-21.3.

13 D. W. Hutmacher, *Scaffolds in Tissue Engineering Bone and Cartilage*, ed. D. F. B. T.-T. B. S. J. C. Williams, Elsevier Science, Oxford, 2000, pp. 175–189, DOI: 10.1016/B978-008045154-1.50021-6.

14 J. Yan, *et al.*, Injectable alginate/hydroxyapatite gel scaffold combined with gelatin microspheres for drug delivery and bone tissue engineering, *Mater. Sci. Eng., C*, 2016, **63**, 274–284, DOI: 10.1016/j.msec.2016.02.071.

15 A. Lueckgen, D. S. Garske, A. Ellinghaus, D. J. Mooney, G. N. Duda and A. Cipitria, Enzymatically-degradable alginate hydrogels promote cell spreading and in vivo tissue infiltration, *Biomaterials*, 2019, **217**, 119294, DOI: 10.1016/j.biomaterials.2019.119294.

16 K. T. Campbell, R. S. Stilhano and E. A. Silva, Enzymatically degradable alginate hydrogel systems to deliver endothelial progenitor cells for potential revasculature applications, *Biomaterials*, 2018, **179**, 109–121, DOI: 10.1016/j.biomaterials.2018.06.038.

17 M. S. Kader, *et al.*, Synthesis and Characterization of BaSO4–CaCO3–Alginate Nanocomposite Materials as Contrast Agents for Fine Vascular Imaging, *ACS Mater. Au*, 2022, **2**(3), 260–268, DOI: **10.1021/acsmaterialsau.1c00070**.

18 F. Ramadhani, L. Miratsi, Z. Humaeroh and F. Afriani, Kemampuan Swelling Hidrogel Berbasis Pva/Alginat, *Proceedings of national colloquium research and community services*, 2021, vol. 5, pp. 149–151, [Online]. Available: **https://journal.ubb.ac.id/index.php/snppm/article/view/2727%0Ahttps://journal.ubb.ac.id/index.php/snppm/article/download/2727/1598**.

19 S. H. Cho, S. M. Lim, D. K. Han, S. H. Yuk, G. Il Im and J. H. Lee, Time-dependent alginate/polyvinyl alcohol hydrogels as injectable cell carriers, *J. Biomater. Sci. Polym. Ed.*, 2009, **20**(7–8), 863–876, DOI: **10.1163/156856209X444312**.

20 A. Espona-Noguera, *et al.*, Tunable injectable alginate-based hydrogel for cell therapy in Type 1 Diabetes Mellitus, *Int. J. Biol. Macromol.*, 2018, **107**, 1261–1269, DOI: **10.1016/j.ijbiomac.2017.09.103**.

21 M. A. Périard, Adverse Effects and Complications Related to the Use of Barium Sulphate Contrast Media for Radiological Examinations of the Gastrointestinal Tract: - A Literature Review -, *Can. J. Med. Radiat. Technol.*, 2003, **34**(3), 3–9, DOI: **10.1016/S0820-5930(09)60005-0**.

22 H. Wang, *et al.*, Injectable hydrogels for spinal cord injury repair, *Eng. Regen.*, 2022, 3(4), 407–419, DOI: **10.1016/j.engreg.2022.09.001**.

23 H. Han, X. Zhao, H. Ma, Y. Zhang and B. Lei, Multifunctional injectable hydrogels with controlled delivery of bioactive factors for efficient repair of intervertebral disc degeneration, *Heliyon*, 2023, **9**(11), e21867, DOI: **10.1016/j.heliyon.2023.e21867**.

24 Y. Zeng, *et al.*, Injectable microcryogels reinforced alginate encapsulation of mesenchymal stromal cells for leak-proof delivery and alleviation of canine disc degeneration, *Biomaterials*, 2015, **59**, 53–65, DOI: **10.1016/j.biomaterials.2015.04.029**.

25 Y.-C. Huang, V. Y. L. Leung, W. W. Lu and K. D. K. Luk, The effects of microenvironment in mesenchymal stem cell–based regeneration of intervertebral disc, *Spine J.*, 2013, **13**(3), 352–362, DOI: **10.1016/j.spinee.2012.12.005**.

26 R. L.-H. Yim, *et al.*, A Systematic Review of the Safety and Efficacy of Mesenchymal Stem Cells for Disc Degeneration: Insights and Future Directions for Regenerative Therapeutics, *Stem Cell. Dev.*, 2014, **23**(21), 2553–2567, DOI: **10.1089/scd.2014.0203**.

27 E. Boelen, L. H. Koole, L. Rhijn and C. Hooy-Corstjens, Towards a functional radiopaque hydrogel for nucleus pulposus replacement, *J. Biomed. Mater. Res. B Appl. Biomater.*, 2007, **83**, 440–450, DOI: **10.1002/jbm.b.30814**.

28 H. Jia, *et al.*, Injectable hydrogel with nucleus pulposus-matched viscoelastic property prevents intervertebral disc degeneration, *J. Orthop. Translat.*, 2022, **33**, 162–173, DOI: **10.1016/j.jot.2022.03.006**.

29 Y. Jiang, *et al.*, A hydrogel reservoir as a self-contained nucleus pulposus cell delivery vehicle for immunoregulation and repair of degenerated intervertebral disc, *Acta Biomater.*, 2023, **170**, 303–317, DOI: **10.1016/j.actbio.2023.08.023**.

30 A. J. Brissenden and B. G. Amsden, In situ forming macroporous biohybrid hydrogel for nucleus pulposus cell delivery, *Acta Biomater.*, 2023, **170**, 169–184, DOI: **10.1016/j.actbio.2023.08.029**.

31 I. Savic Gajic, I. Savic and Z. Svirčev, Preparation and Characterization of Alginate Hydrogels with High Water-Retaining Capacity, *Polymers*, 2023, **15**, 2592, DOI: **10.3390/polym15122592**.

32 Y. Li, J. Rodrigues and H. Tomás, Injectable and biodegradable hydrogels: gelation. biodegradation and biomedical applications, *Chem. Soc. Rev.*, 2012, **41**(6), 2193–2221, DOI: **10.1039/C1CS15203C**.

33 X. Wang, *et al.*, Injectable silk-polyethylene glycol hydrogels, *Acta Biomater.*, 2015, **12**, 51–61, DOI: **10.1016/j.actbio.2014.10.027**.

34 K. L. Spiller, S. J. Laurencin and A. M. Lowman, Characterization of the behavior of porous hydrogels in model osmotically-conditioned articular cartilage systems, *J. Biomed. Mater. Res. B Appl. Biomater.*, 2009, **90**(2), 752–759, DOI: **10.1002/jbm.b.31344**.

35 K. Zhang, W. Feng and C. Jin, Protocol efficiently measuring the swelling rate of hydrogels, *MethodsX*, 2020, 7, 100779, DOI: **10.1016/j.mex.2019.100779**.

36 M. J. de Lima Brossi, D. J. Jiménez, L. Cortes-Tolalpa and J. D. van Elsas, Soil-Derived Microbial Consortia Enriched with Different Plant Biomass Reveal Distinct Players Acting in Lignocellulose Degradation, *Microb. Ecol.*, 2016, **71**(3), 616–627, DOI: **10.1007/s00248-015-0683-7**.

37 S. Gorgieva and V. Kokol, Preparation. characterization. and in vitro enzymatic degradation of chitosan-gelatine hydrogel scaffolds as potential biomaterials, *J. Biomed. Mater. Res., Part A*, 2012, **100**(7), 1655–1667, DOI: **10.1002/jbm.a.34106**.

38 C. K. Kuo and P. X. Ma, Ionically crosslinked alginate hydrogels as scaffolds for tissue engineering: Part 1. Structure. gelation rate and mechanical properties, *Biomaterials*, 2001, **22**(6), 511–521, DOI: **10.1016/S0142-9612(00)00201-5**.

39 R. Tan, X. Niu, S. Gan and Q. Feng, Preparation and characterization of an injectable composite, *J. Mater. Sci. Mater. Med.*, 2009, **20**(6), 1245–1253, DOI: **10.1007/s10856-009-3692-6**.

40 A. Yumin, D. Liguo, Y. Yi and J. Yongna, Mechanical properties of an interpenetrating network poly(vinyl alcohol)/alginate hydrogel with hierarchical fibrous structures, *RSC Adv.*, 2022, **12**(19), 11632–11639, DOI: **10.1039/D1RA07368K**.

41 Y. Zhang, *et al.*, Characterization and cytocompatibility of 3D porous biomimetic scaffold derived from rabbit nucleus pulposus tissue in vitro, *J. Mater. Sci. Mater. Med.*, 2021, **32**(1), 8, DOI: **10.1007/s10856-020-06480-9**.

42 W. Gao, B. Zhou, X. Ma, Y. Liu, Z. Wang and Y. Zhu, Preparation and characterization of BaSO4/poly(ethylene terephthalate) nanocomposites, *Colloids Surf., A*, 2011, **385**(1), 181–187, DOI: **10.1016/j.colsurfa.2011.06.015**.

43 A. G. Hadi, *et al.*, Study the Effect of Barium Sulphate on Optical Properties of Polyvinyl Alcohol (PVA), *Univers. J. Mater. Sci.*, 2013, **1**(2), 52–55, DOI: **10.13189/ujms.2013.010207**.

44 M. B. Nair, G. Baranwal, P. Vijayan, K. S. Keyan and R. Jayakumar, Composite hydrogel of chitosan–poly(hydroxybutyrate-co-valerate) with chondroitin sulfate nanoparticles for nucleus pulposus tissue engineering, *Colloids Surf., B*, 2015, **136**, 84–92, DOI: **10.1016/j.colsurfb.2015.08.026**.

45 N. Newell, J. P. L. A. Christou, M. A. Adams, C. J. Adam and S. D. Masouros, Biomechanics of the human intervertebral disc: A review of testing techniques and results, *J. Mech. Behav. Biomed. Mater.*, 2017, **69**, 420–434, DOI: **10.1016/j.jmbbm.2017.01.037**.

46 Q. Wang, *et al.*, X-ray Visible and Uniform Alginate Microspheres Loaded with in Situ Synthesized BaSO4 Nanoparticles for in Vivo Transcatheter Arterial Embolization, *Biomacromolecules*, 2015, **16**(4), 1240–1246, DOI: **10.1021/acs.biomac.5b00027**.

47 A. Kroll, *et al.*, Cytotoxicity screening of 23 engineered nanomaterials using a test matrix of ten cell lines and three different assays, *Part. Fibre Toxicol.*, 2011, **8**, 9, DOI: **10.1186/1743-8977-8-9**.

48 C. E. Dallas and P. L. Williams, Barium: rationale for a new oral reference dose, *J. Toxicol. Environ. Health B Crit. Rev.*, 2001, **4**(4), 395–429, DOI: **10.1080/109374001753146216**.

49 N. Kamaly, B. Yameen, J. Wu and O. C. Farokhzad, Degradable Controlled-Release Polymers and Polymeric Nanoparticles: Mechanisms of Controlling Drug Release, *Chem. Rev.*, 2016, **116**(4), 2602–2663, DOI: **10.1021/acs.chemrev.5b00346**.

50 D. R. Barleany, F. Ulfiyani, S. Istiqomah, H. H. Rahmayetty and E. Erizal, Swelling properties of cassava starch grafted with poly (potassium acrylate-co-acrylamide) superabsorbent hydrogel prepared by ionizing radiation, *AIP Conf. Proc.*, 2015, **1699**, 040008, DOI: **10.1063/1.4938323**.

51 E. Erizal, D. P. Perkasa, B. Abbas, S. Sudirman and G. S. Sulistioso, Fast swelling superabsorbent hydrogels starch based prepared by gamma radiation techniques, *Indones. J. Chem.*, 2014, **14**(3), 246–252, DOI: **10.22146/ijc.21235**.